Supplementary Information

Scalable and green formation of graphitic nanolayers produces highly conductive pyrolyzed paper toward sensitive electrochemical sensors

Marcos V. de Lima Tinoco,[#a] Lucas R. Fujii,[#a,b] Caroline Y. N. Nicoliche,[a] Gabriela F. Giordano,[a] Julia A. Barbosa,[a,c] Jaqueline F. da Rocha,[a,d] Gabriel T. dos Santos,[a,e] Jefferson Bettini,[a] Murilo Santhiago,[a,d] Mathias Strauss,*[a] and Renato S. Lima*[a,b,c,d]

[a]Brazilian Nanotechnology National Laboratory, Brazilian Center for Research in Energy and Materials, Campinas, São Paulo 13083-970, Brazil
[b]Institute of Chemistry, University of Campinas, Campinas, São Paulo 13083-970, Brazil
[c]São Carlos Institute of Chemistry, University of São Paulo, São Carlos, São Paulo 13566-590, Brazil
[d]Center for Natural and Human Sciences, Federal University of ABC, Santo André, São Paulo 09210-580, Brazil
[e]Material Science, Federal University of Rio Grande do Sul, Porto Alegre, Rio Grande do Sul 90010-150, Brazil
*Corresponding authors: mathias.strauss@lnnano.cnpem.br and renato.lima@lnnano.cnpem.br

This Supplementary Information includes:

▪ **Supporting text**

▪ **Supporting tables**

▪ **Supporting figures**

▪ **Movie caption**

▪ **References**

Supporting text

1. Resistivity measurements

Gold thin film-based fingers were used as pads for measuring the resistance of pyrolyzed paper (PP) strips. These fingers were obtained by photolithography routines.[1] Thin films of Cr (20 nm) and Au (110 nm) were deposited via sputtering (Balzers BA510) on glass, making a total of 16 pads with 4.0 mm gap and width and 1.0 mm length. Resistances (R) were recorded using a multimeter (Minipa, Model ET-2652). Specifically, the values of R were collected at each 4 mm until the total distance of 6 cm. After, the curve R *vs* length was plotted from which the resistivity (ρ) was obtained taking the curve slope through the following **Equation S2**, with A meaning the electrode cross-sectional area.

$$\rho = \text{slope. A} \qquad\qquad \textbf{(Equation S1)}$$

2. Factorial design

First, we performed an initial exploration with a Factorial Design 2^3 to verify the effects and the contribution of each factor on ρ, namely, pyrolysis temperature (PT), annealing temperature (AT), and presence of isopropanol atmosphere during annealing step (IP). From this analysis, the IP factor showed to have the greatest contribution to the reduction of resistivity. Then, we refined the design working on the high level (1000 °C) of the IP factor. In this scenery, the AT drastically affects the resistivity reduction. Thereby, based on the effects of PT, AT and their mutual interaction, the **Equation S2** was attained and, then used to simulate the data of resistivity with Box-Wilson central composite design (CCD) start points.

$$\rho = 33.9 - 5.6x_1 - 24.6x_2 \qquad\qquad \textbf{(Equation S2)}$$

The F-test was used to compare the variances by the ratio of the values of *F* and $F_{tab.}$ as shown in ANOVA (**Table S3**). The calculated *F* value for the regression is almost 40 times higher than $F_{tab(\alpha=0.05)}$, meaning that the means squares of regression and residual are statistically different on each other and ultimately the unmodeled information (lack of fit) is not confused with modeled (regression) information, with no pattern or tendency being observed. To date, the residual values were homocedastics.[2,3]

Other important result provided from ANOVA is the *F* value for the pure error by allowing us for comparing the means squares of lack of fit and pure error obtained from the triplicate at the central point (900 °C). This *F* value for the pure error was notably lower than $F_{tab(\alpha=0.05)}$, indicating that the information unmodeled by the regression could be assigned to the random experimental error.[2–4]

3. Procedure to quantify the PP graphitization through EELS data

The method to characterize the graphitization considers the intensity relationship between three fitted peaks in the energy electron loss spectroscopy (EELS) spectra. All spectra in the EELS data cube were aligned using π^* peak to minimize the energy difference between pixels. Importantly, an 866 GIF Tridiem was used to obtain EELS data. Continuing, the first peak was defined by the position of the π^* peak, whereas the original σ peak was deconvoluted into two peaks, namely, σ^* and σ_1. These peaks were defined by fixed energy differences of 6.7 (σ^*) and 13.7 eV (σ_1) greater than the π^* peak (see **Fig. S5**). The graphitization index (G_i) was defined by the **Equation S3**. The value found for the graphite EELS standard was 0.803 and the value found for the raw paper EELS standard was 0.602. These values composed the temperature-color scale thresholds (i.e., maximum and minimum; see **Fig. 4C**).

$$G_i = \left[\frac{(\pi^* \times \sigma^*)}{(\sigma_1)^2} \right] \qquad\qquad \textbf{(Equation S3)}$$

4. Heterogeneous standard rate constant calculation

Cyclic voltammetry (CV) and electrochemical impedance spectroscopy (EIS) analyses were performed in a three-electrode system using PP as the working electrode, a platinum wire (1 cm²) as the counter electrode, and Ag/AgCl (Metrohm, 3.0 mol L^{-1} KCl) as reference electrode. The redox probe 1.0 mmol L^{-1} [Fe(CN)$_6$]$^{3/4-}$ was diluted into 1.0 mol L^{-1} KCl (supporting electrolyte). Voltammograms were registered at different scan rates (10, 20, 40, 60, 80, and 100 mV s^{-1}). Three cycles from –0.05 V to +0.55 V *vs* Ag/AgCl were made at each scan rate. To calculate the heterogeneous standard rate constant (k$_0$), the dimensionless kinetic parameter of Nicholson, ψ, was obtained from the **Equation S4** as proposed by Lavagnini *et al.*:[5]

$$\psi = \frac{(-0.6288 + 0.0021\,(n\Delta E_p))}{(1 - 0.017(n\Delta E_p))} \qquad \textbf{(Equation S4)}$$

in which n is the number of electrons involved in the reversible redox reaction and ΔE_p is the peak-to-peak potential separation of the anodic and cathodic current peaks. From the slope of the plot ψ *vs* [πDnF/(RT)] v$^{-1/2}$ and considering the diffusion coefficient, D, of the reduction of [Fe(CN)$_6$]$^{3-}$ as 6.7 10^{-6} cm^2 s^{-1} at 25 °C (i.e., πDnF/(RT) = 34.94),[6] the kinetic parameter, k$_0$, could be calculated.[7]

5. Loss of water contents

The relative water contents (RWC) were acquired according to the **Equation S5**. In this equation, the initial turgid (w$_{hydrated}$) and dry (w$_{dry}$) masses of soy leaves were obtained as reported in our previous work.[8] Briefly, an excessive hydration of the plant was accomplished from its root during 24 h to obtain w$_{hydrated}$. To acquire w$_{dry}$, in turn, the leaves were placed into an oven at 60 °C for 1 h. By using the **Equation S6**, RWC could be converted into the loss of water contents (LWC).

$$\text{RWC (\%)} = \frac{w_{fresh} - w_{dry}}{w_{hydrated} - w_{dry}} * 100 \qquad \textbf{(Equation S5)}$$

$$\text{LWC (\%)} = 100 - \text{RWC} \qquad \textbf{(Equation S6)}$$

Supporting tables

Table S1. Coefficients obtained by the regression

	$\bar{b}$	$\bar{b} - CI$	$\bar{b} + CI$	CI^a
b$_0$	23.3	19.6	27.0	3.7
b$_1$	-5.8	-8.1	-3.6	2.3
b$_2$	-24.0	-26.3	-21.7	2.3
b$_1{}^2$	5.3	2.6	8.0	2.7
b$_2{}^2$	5.8	3.1	8.5	2.7
b$_{12}$	4.2	1.0	7.4	3.2

^{a}Confidence Interval.

Table S2. Experimental design of CCD

Experiment	b_1 = PT		b_2 = AT		ρ (mΩ.cm)
	Real	Normalized	Real	Normalized	
1	800.0	-1.0	800.0	-1.0	75.3
2	1000.0	1.0	800.0	-1.0	43.7
3	800.0	-1.0	1000.0	1.0	10.4
4	1000.0	1.0	1000.0	1.0	9.5
5	900.0	0.0	900.0	0.0	24.3
6	900.0	0.0	900.0	0.0	19.3
7	900.0	0.0	900.0	0.0	26.3
8	758.6	-1.4	900.0	0.0	41.8
9	900.0	0.0	758.6	-1.4	68.7
10	1041.4	1.4	900.0	0.0	26.0
11	900.0	0.0	1041.4	1.4	1.0

Table S3. Analysis of variance (ANOVA) of the regression and pure error shown

Parameter	SS[a]	df[b]	MS[c]	F	$F_{tab. (\alpha=0.05)}$	F-test[d]
Regression	5221.30	5.00	1044.30	196.60	5.05	38.82
Residuals	26.56	5.00	5.31			
Total	5247.90	10.00	524.79			
Pure Error	26.04	2.00	13.02	0.013	19.16	0.00068
Lack of fit	0.52	3.00	0.17			
R^2	0.99	1.00				
$R^2_{Máx}$	0.995	1.00				

[a]Sum of squares, [b]degrees of freedom, [c]mean square, [d]F /F$_{tab}$.

Table S4. Roughness values and the ensuing standard deviations for each sample

Sample	Roughness (μm)
PP^8	0.46 ± 0.30
PP^8_{I8}	0.29 ± 0.10
PP^{10}_{N10}	0.28 ± 0.06
PP^8_{N10}	0.27 ± 0.12
PP^{10}_{I10}	0.24 ± 0.09
PP^8_{I10}	0.19 ± 0.07

Table S5. Capacitive gradient data of replicates at 3 different regions of each PP and the ensuing average value

Sample	Replicates			Avg. dC/dZ
PP^8_{I10}	25.0	25.34	25.38	24.74 ± 0.64
PP^8	20.5	21.9	22.3	21.57 ± 0.77

Table S6. Elongation at the ruptures (Er) and the resulting standard deviations for each sample

Sample	Er (mm)
PP_{N10}^{10}	10.82 ± 0.36
PP^{10}	10.09 ± 0.45
PP_{N10}^{8}	9.85 ± 0.21
PP^{8}	8.69 ± 1.53
PP_{I10}^{8}	5.96 ± 1.82
PP_{I10}^{10}	4.59 ± 0.37

Table S7. Modulus of elasticity and the resulting standard deviations for each sample

Sample	Modulus of Elasticity (MPa)
PP_{I10}^{10}	426.09 ± 61.04
PP_{N10}^{8}	288.31 ± 17.50
PP_{I10}^{8}	147.97 ± 13.39
PP_{N10}^{10}	141.07 ± 16.88
PP^{10}	119.06 ± 17.06
PP^{8}	98.07 ± 15.58

Table S8. I_D/I_G ratios and the ensuing standard deviations for each sample

Sample	I_D/I_G ratio
PP_{I10}^{10}.	1.80 ± 0.044
PP_{I10}^{8}	1.73 ± 0.237
PP^{10}	1.63 ± 0.100
PP_{N10}^{8}	1.53 ± 0.011
PP_{N10}^{10}	1.52 ± 0.027
PP^{8}	1.36 ± 0.016

Table S9. Values of k^0 reported in the literature for different electrode materials

Electrode	k^0 (cm s^{-1})
Pyrolyzed paper with cellulose acetate[9]	$1.5 \; 10^{-3}$
Reduced graphene oxide foam[10]	$2.4 \; 10^{-4}$
Commercially screen-printed carbon[11,12]	$*1.09 \; 10^{-3}$ $**3.08 \; 10^{-3}$
Commercially boron-doped diamond[11]	$3.62 \; 10^{-3}$
Commercially glassy carbon[11]	$4.60 \; 10^{-3}$
Commercially pencil graphite[11]	$3.02 \; 10^{-3}$
Carbon paper[11]	$1.6 \; 10^{-3}$
Graphite powder with nail polish[12]	$5.82 \; 10^{-3}$
ITO[12]	$2.57 \; 10^{-3}$

The values highlighted by the symbols * and ** are related to the references 11 and 12, respectively.
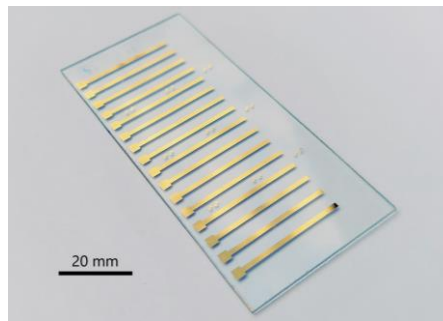
Supporting figures

Fig. S1. Digital image of gold thin film-based fingers fabricated by photolithography for measuring the PP resistances.
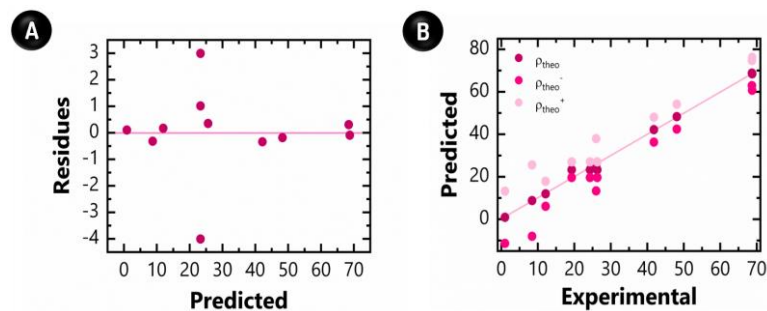

Fig. S2. Results obtained from ANOVA. **(A)** Plot of residual analysis. **(B)** Predicted values of resistivity as a function of the experimental values.
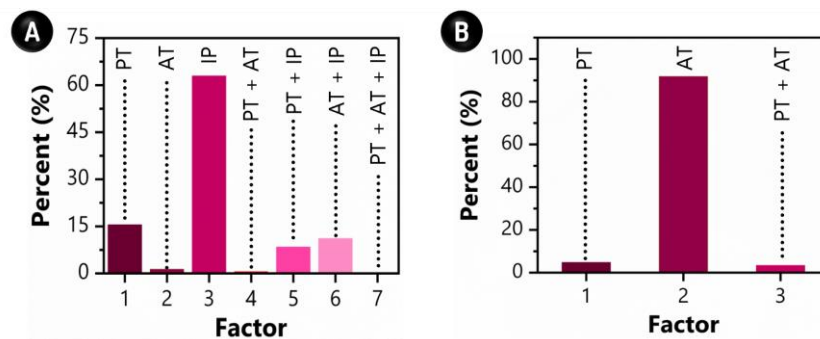

Fig. S3. Percentage contributions of the factors on the resistivity according to factorial design. **(A)** Individual factors, i.e., PT, AT, and IP, and their interactions. **(B)** Factors PT, AT, and their interaction considering the high level of IP.
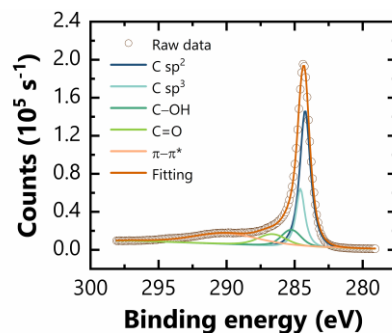
Fig. S4. Carbon high-resolution spectrum reached through X-ray photoelectron spectroscopy (XPS) of a silicon piece that was placed into furnace along isopropanol-vapor annealing at 1000 °C.
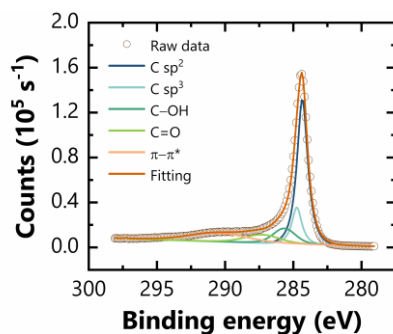
Fig. S5. Carbon high-resolution spectrum obtained by XPS of PP prepared by annealing under ethanol vapor at 1000 °C.
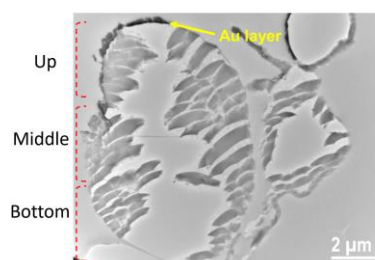

Fig. S6. Transmission electron microscopy (TEM) image of a PP sample highlighting the Au thin film sputtered on PP surface. This step was intended to identify the PP top in the microscope. The regions of the PP, i.e., up, middle, and bottom, are also illustrated in this image.
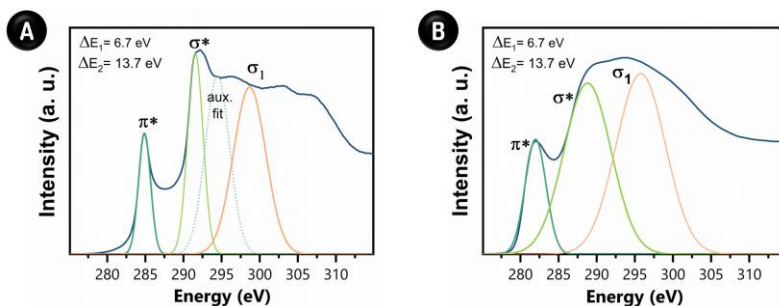

Fig. S7. EELS data. Typical graphs for **(A)** graphite and **(B)** raw paper. Both these graphs exhibit the gaussian peak fits and the corresponding energy difference among them.
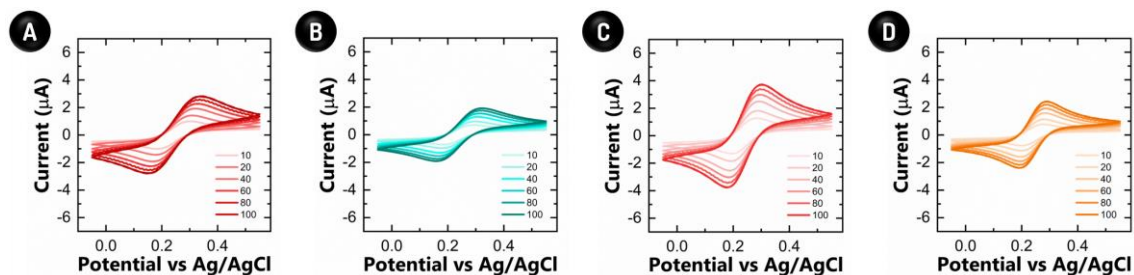

Fig. S8. Cyclic voltammograms to 1.0 mmol L^{-1} [Fe(CN)$_6$]$^{4/3-}$ at different scan rates (mV s^{-1}) as highlighted. These data were achieved for the electrodes **(A)** PP$_{N10}^{8}$, **(B)** PP^{10}, **(C)** PP$_{N10}^{10}$, and **(D)** PP$_{I10}^{10}$.
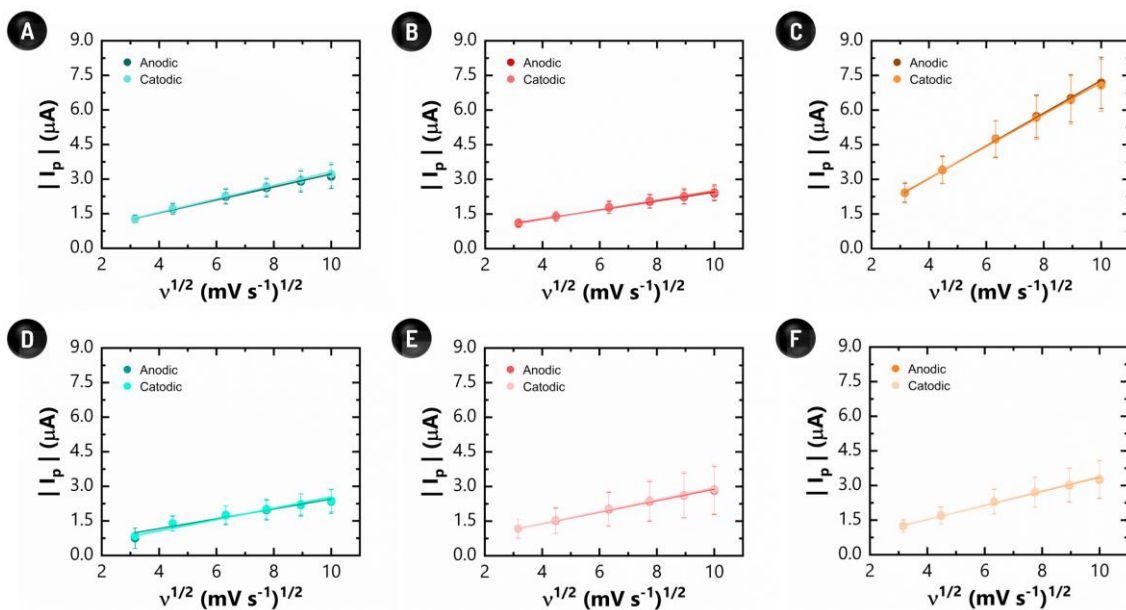
Fig. S9. Module of peak currents, anodic and cathodic, as a function of the square root of scan rate. These data were achieved for the electrodes **(A)** PP^8, **(B)** PP^8_{N10}, **(C)** PP^8_{I10}, **(D)** PP^{10}, **(E)** PP^{10}_{N10}, and **(F)** PP^{10}_{I10}.
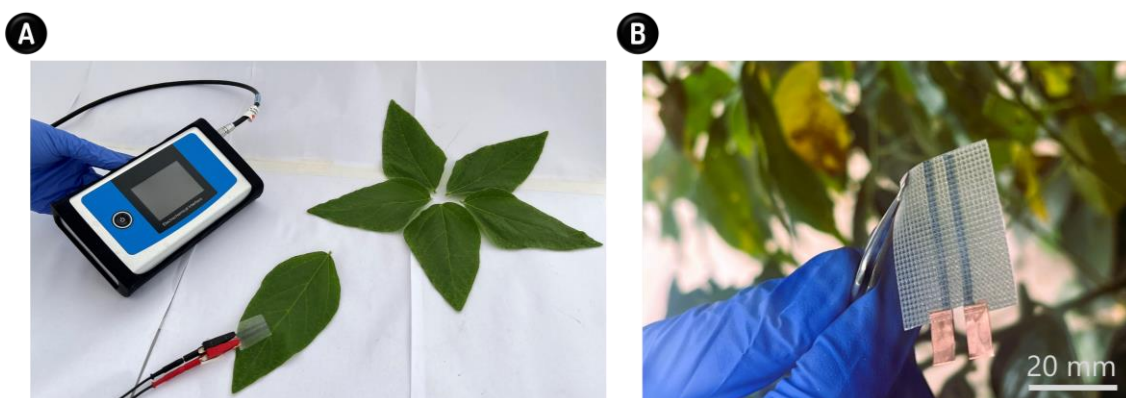

Fig. S10. Digital images of the on-leaf system. **(A)** Platform consisting of electrodes and a portable potentiostat. **(B)** Electrodes with attached copper pads and adhesive tape.
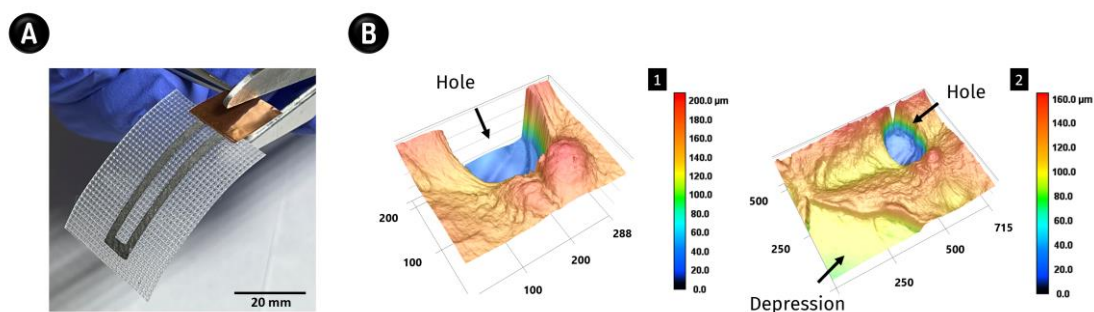

Fig. S11. Details regarding the adhesive tape used to fix the electrodes onto soy leaves. **(A)** Digital image showing the procedure of cutting a copper adhesive tape-based pad and underlying PP. Such a step was intended to allow electrical contact of the on-leaf electrodes to the potentiostat. **(B)** Images obtained by laser scanning confocal microscopy (LSCM) highlighting the holes and a low-relief region of the adhesive tape.
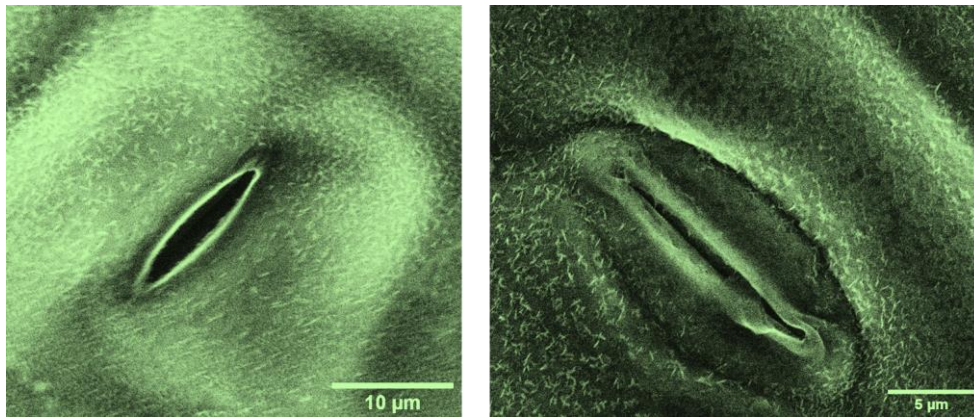
Fig. S12. Environmental scanning electron microscopy (ESEM) images of stomata over a typical soy leaf surface.

Movie caption

Video S1. Fabrication of PP patterns using a knife plotter and images of the final adhesive tape-stuck electrodes toward on-leaf measurements.

References

1   L. F. Ferreira, G. F. Giordano, A. L. Gobbi, M. H. O. Piazzetta, G. R. Schleder and R. S. Lima, *ACS Sens.*, 2022, **7**, 1045–1057.

2   D. C. Montgomery, G. C. Runger and N. F. Hubele, *Engineering statistics*, John Wiley & Sons, 2009.

3   E. R. Pereira Filho, *Planejamento fatorial em química: maximizando a obtenção de resultados*, EdUFScar: *São Carlos, SP, 2014*.

4   F. Pereira and E. Pereira-Filho, *Quim. Nova*, 2018, **41**, 1061–1071.

5   I. Lavagnini, R. Antiochia and F. Magno, *Electroanalysis*, 2004, **16**, 505–506.

6   S. J. Konopka and B. McDuffie, *Anal. Chem.*, 1970, **42**, 1741–1746.

7   R. S. Nicholson and I. Shain, *Anal. Chem.*, 1964, **36**, 706–723.

8   J. A. Barbosa, V. M. S. Freitas, L. H. B. Vidotto, G. R. Schleder, R. A. G. de Oliveira, J. F. da Rocha, L. T. Kubota, L. C. S. Vieira, H. C. N. Tolentino, I. T. Neckel, A. L. Gobbi, M. Santhiago and R. S. Lima, *ACS Appl. Mater. Interfaces*, 2022, **14**, 22989–23001.

9   S. Damasceno, C. C. Corrêa, R. F. Gouveia, M. Strauss, C. C. B. Bufon and M. Santhiago, *Adv. Electron. Mater.*, 2020, **6**, 1900826.

10   L. Baptista-Pires, A. de la Escosura-Muniz, M. Balsells, J. C. Zuaznabar-Gordona, A. Merkoçi, *Electrochem Commun*, 2019, **98**, 6–9.

11   Á. Torrinha, M. Martins, M. Tavares, C. Delerue-Matos and S. Morais, *Talanta*, 2021, **226**, 122111.

12   L. F. de Lima, A. L. Ferreira, C. C. Maciel, M. Ferreira and W. R. de Araujo, *Talanta*, 2021, **227**, 122200.